Sum-Rule Conserving Spectral Functions from the Numerical Renormalization Group

Andreas Weichselbaum and Jan von Delft

Physics Department, Arnold Sommerfeld Center for Theoretical Physics, and Center for NanoScience, Ludwig-Maximilians-Universität München, D-80333 München, Germany

(Received 1 August 2006; published 16 August 2007)

We show how spectral functions for quantum impurity models can be calculated very accurately using a complete set of discarded numerical renormalization group eigenstates, recently introduced by Anders and Schiller. The only approximation is to judiciously exploit energy scale separation. Our derivation avoids both the overcounting ambiguities and the single-shell approximation for the equilibrium density matrix prevalent in current methods, ensuring that relevant sum rules hold rigorously and spectral features at energies below the temperature can be described accurately.

DOI: 10.1103/PhysRevLett.99.076402 PACS numbers: 71.27.+a, 73.21.La, 75.20.Hr

Quantum impurity models describe a quantum system with a small number of discrete states, the ''impurity,'' coupled to a continuous bath of fermionic or bosonic excitations. Such models are relevant for describing transport through quantum dots, for the treatment of correlated lattice models using dynamical mean field theory, or for the modeling of the decoherence of qubits.

The impurity's dynamics in thermal equilibrium can be characterized by spectral functions of the type $\mathcal{A}^{\mathcal{BC}}(\omega) = \int \frac{dt}{2\pi} e^{i\omega t}\langle \hat{\mathcal{B}}(t)\hat{\mathcal{C}}\rangle_T$. Their Lehmann representation reads

$$\mathcal{A}^{\mathcal{BC}}(\omega) = \sum_{a,b} \langle b|\hat{\mathcal{C}}|a\rangle \frac{e^{-\beta E_a}}{Z} \langle a|\hat{\mathcal{B}}|b\rangle \delta(\omega - E_{ba}), \quad (1)$$

with $Z = \sum_a e^{-\beta E_a}$ and $E_{ba} = E_b - E_a$, which implies the sum rule $\int d\omega \mathcal{A}^{\mathcal{BC}}(\omega) = \langle \hat{\mathcal{B}}\hat{\mathcal{C}}\rangle_T$. In this Letter, we describe a strategy for numerically calculating $\mathcal{A}^{\mathcal{BC}}(\omega)$ that, in contrast to previous methods, rigorously satisfies this sum rule and accurately describes both high *and* low frequencies, including $\omega \lesssim T$, which we test by checking our results against exact Fermi-liquid relations.

Our work builds on Wilson's numerical renormalization group (NRG) method [1]. Wilson discretized the environmental spectrum on a logarithmic grid of energies Λ^{-n} (with $\Lambda > 1$, $1 \le n \le N \to \infty$), with exponentially high resolution of low-energy excitations, and mapped the impurity model onto a ''Wilson tight-binding chain,'' with hopping matrix elements that decrease exponentially as $\Lambda^{-n/2}$ with site index n. Because of this separation of energy scales, the Hamiltonian can be diagonalized iteratively: adding one site at a time, a new ''shell'' of eigenstates is constructed from the new site's states and the M_K lowest-lying eigenstates of the previous shell (the so-called ''kept'' states), while ''discarding'' the rest.

Subsequent authors [2–10] have shown that spectral functions such as $\mathcal{A}^{\mathcal{BC}}(\omega)$ can be calculated via the Lehmann sum, using NRG states (kept and discarded) of those shells n for which $\omega \sim \Lambda^{-n/2}$. Though plausible on heuristic grounds, this strategy entails double-counting ambiguities [5] about how to combine data from successive shells. Patching schemes [9] for addressing such ambiguities involve arbitrariness. As a result, the relevant sum rule is not satisfied rigorously, with typical errors of a few percent. Also, the thermal density matrix (DM) $\hat{\rho} = e^{-\beta\hat{H}}/Z$ has until now been represented rather crudely using only the single N_Tth shell for which $T \simeq \Lambda^{-1/2(N_T-1)}$ [8], with a chain of length $N = N_T$, resulting in inaccurate spectral information for $\omega \lesssim T$. In this Letter we avoid these problems by using in the Lehmann sum an approximate but *complete* set of eigenstates, introduced recently by Anders and Schiller (AS) [11].

Wilson's truncation scheme.—The Wilson chain's zeroth site represents the bare impurity Hamiltonian $\hat{h}_0$ with a set of d_0 impurity states $|\sigma_0\rangle$. It is coupled to a fermionic chain, whose nth site ($1 \le n \le N$) represents a set of d states $|\sigma_n\rangle$, responsible for providing energy resolution to the spectrum at scale $\Lambda^{-n/2}$. For a spinful fermionic band, for example, $\sigma_n \in \{0, \uparrow, \downarrow, \uparrow\downarrow\}$, hence $d = 4$. (Bosonic chains can be treated similarly [10].) The Hamiltonian $\hat{H} = \hat{H}_N$ for the full chain is constructed iteratively by adding one site at a time, using $\hat{H}_n = \hat{H}_{n-1} + \hat{h}_n$ (acting in a $d^n d_0$-dimensional Fock space $\mathcal{F}_n$ spanned by the basis states $\{|\sigma_n\rangle \otimes \cdots \otimes |\sigma_0\rangle\}$), where $\hat{h}_n$ links sites n and $n-1$ with hopping strength $\sim\Lambda^{-n/2}$. Since the number of eigenstates of $\hat{H}_n$ grows exponentially with n, Wilson proposed the following iterative truncation scheme to numerically diagonalize the Hamiltonian: Let n_0 be the last iteration for which a complete set $\{|s\rangle_{n_0}^K\}$ of kept eigenstates of $\hat{H}_{n_0}$ can be calculated without trunction. For $n > n_0$, construct the orthonormal eigenstates $\{|s\rangle_n^X\}$ of $\hat{H}_n$ (the nth ''shell''), with eigenvalues E_s^n, as linear combinations of the kept eigenstates $|s\rangle_{n-1}^K$ of $\hat{H}_{n-1}$ and the states $|\sigma_n\rangle$ of site n,

$$|s'\rangle_n^X = \sum_{\sigma_n s}^{K} |\sigma_n\rangle \otimes |s\rangle_{n-1}^K [A_{KX}^{[\sigma_n]}]_{ss'}, \quad (2)$$

with coefficients arranged into a matrix $A_{KX}^{[\sigma_n]}$ whose ele-

ments are labeled by ss'. The superscript $X = K$ or D indicates that the new shell has been partitioned into "kept" states (say the M_K lowest-lying eigenstates of $\hat{H}_n$) to be retained for the next iteration and "discarded" states (the remaining ones). Since $\hat{h}_n$ acts as a weak perturbation (of relative size $\Lambda^{-1/2}$) on $\hat{H}_{n-1}$, the d-fold degeneracy of the states $|\sigma_n\rangle \otimes |s\rangle^X_{n-1}$ is lifted, resulting in a characteristic energy spacing $\Lambda^{-n/2}$ for shell n. Iterating until the spectrum of low-lying eigenvalues has reached a fixed point (for $n = N$, say), one generates a set of eigenstates $\{|s\rangle^X_n\}$ with the structure of matrix product states [12] (Fig. 1). The states generated for the last Nth shell will all be regarded as discarded [11].

Anders-Schiller basis.—Recently, AS have shown [11] that the discarded states can be used to build a complete basis for the whole Wilson chain: the states $\{|s\rangle^X_n\}$ describing the nth shell are supplemented by a set of d^{N-n} *degenerate* "environmental" states $\{|e_n\rangle = |\sigma_N\rangle \otimes \cdots \otimes |\sigma_{n+1}\rangle\}$ spanning the rest of the chain to construct the set of states $\{|se\rangle^X_n \equiv |e_n\rangle \otimes |s\rangle^X_n\}$. These reside in the complete Fock space $\mathcal{F}_N$ of the full chain, spanning $\mathcal{F}_N$ if $n \le n_0$. Ignoring the degeneracy-lifting effect of the rest of the chain, these states become approximate eigenstates of the Hamiltonian $\hat{H}_N$ of the *full* chain ("NRG approximation"),

$$\hat{H}_N|se\rangle^X_n \simeq E^n_s|se\rangle^X_n, \tag{3}$$

with eigenenergies *independent* of the (d^{N-n})-fold degenerate environmental index e_n. (This will facilitate tracing out the environment below.) By construction, we have ${}^D_m\langle se|s'e'\rangle^D_n = \delta_{mn}\delta_{e_n e'_n}\delta_{ss'}$ and

$${}^K_m\langle se|s'e'\rangle^D_n = \begin{cases} 0, & m \ge n \\ \delta_{e_n e'_n}[A^{\sigma_{m+1}}_{KK}\ldots A^{\sigma_n}_{KD}]_{ss'}, & m < n. \end{cases} \tag{4}$$

The discarded states of shell n are orthogonal to the discarded states of any other shell, and to the kept states of that or any later shell. Combining the discarded states from all shells thus yields a complete set of NRG eigenstates of $\hat{H}_N$, the "Anders-Schiller basis," that span the full Fock space $\mathcal{F}_N$ ($\sum_n$ henceforth stands for $\sum_{n>n_0}^N$):

$$\mathbf{1}^{(d_0 d^N)} = \sum_{se} |se\rangle^K_{n_0\,n_0}\langle se| = \sum_n \sum_{se} |se\rangle^D_{n\,n}\langle se|. \tag{5}$$

Local operators.—Let us now consider a "local" operator $\hat{\mathcal{B}}$ acting nontrivially only on sites up to n_0. Two

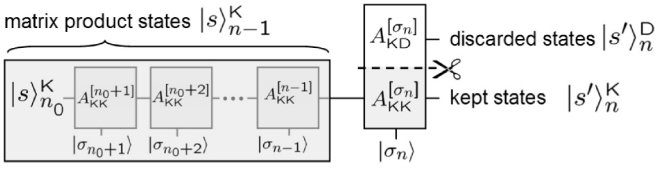

FIG. 1. Diagram for the kept (or discarded) matrix product state $|s'\rangle^K_n$ (or $|s'\rangle^D_n$): the nth box represents the matrix block $A^{[\sigma_n]}_{KX}$, its left, bottom, and right legs carry the labels of the states $|s\rangle^K_{n-1}$, $|\sigma_n\rangle$, and $|s'\rangle^K_n$ (or $|s'\rangle^D_n$), respectively.

particularly useful representations are

$$\hat{\mathcal{B}} = \sum_{ss'e} |se\rangle^K_{n_0}[\mathcal{B}^{[n_0]}_{KK}]_{ss'}{}^K_{n_0}\langle s'e| = \sum_n \sum_{XX'}^{\neq KK} \hat{\mathcal{B}}^{[n]}_{XX'}. \tag{6}$$

The left equality, written $\hat{\mathcal{B}} = \hat{\mathcal{B}}^{[n_0]}_{KK}$ in brief, represents the operator in the complete basis set $\{|se\rangle^K_{n_0}\}$, with matrix elements known exactly numerically (possibly up to fermionic minus signs depending on the environmental states, but these enter quadratically in correlation functions and hence cancel). The right-hand side (RHS) of Eq. (6) expresses $\hat{\mathcal{B}}$ in the AS basis and is obtained as follows: starting from $\hat{\mathcal{B}}^{[n_0]}_{KK}$, one iteratively refines the "kept-kept" part of $\hat{\mathcal{B}}$ from, say, the $(n-1)$th iteration in terms of the NRG eigenstates $\{|se\rangle^x_n\}$ of the next shell, including both kept and discarded states ($X = K, D$),

$$\hat{\mathcal{B}}^{[n-1]}_{KK} = \sum_{XX'}\sum_{ss'e} |se\rangle^X_n[\mathcal{B}^{[n]}_{XX'}]_{ss'}{}^{X'}_n\langle s'e| = \sum_{XX'} \hat{\mathcal{B}}^{[n]}_{XX'}, \tag{7}$$

thereby defining the operators $\hat{\mathcal{B}}^{[n]}_{XX'}$, with matrix elements $[\mathcal{B}^{[n]}_{XX'}]_{ss'} = [A^{[\sigma_n]\dagger}_{XK}\mathcal{B}^{[n-1]}_{KK}A^{[\sigma_n]}_{KX'}]_{ss'}$. Splitting off all $XX' \neq KK$ terms (DD, KD, DK) and iteratively refining each KK term until $n = N$, we obtain the RHS of Eq. (6). It has two important features. First, the matrix elements of the time-dependent operator $\hat{\mathcal{B}}(t) = e^{i\hat{H}t}\hat{\mathcal{B}}e^{-i\hat{H}t}$, evaluated within the NRG approximation, $[\mathcal{B}^{XX'}_n(t)]_{ss'} \simeq [\mathcal{B}^{XX'}_n]_{ss'}e^{it(E^n_s - E^n_{s'})}$, contain differences of eigenenergies from the *same* shell only, i.e., calculated with the same level of accuracy. Second, by *excluding* KK terms it rigorously avoids the double-counting ambiguities and heuristic patching rules plaguing previous approaches [2–10].

Thermal averages.—To calculate thermal averages $\langle\ldots\rangle_T = \mathrm{Tr}[\hat{\rho}\ldots]$, we write the full density matrix (FDM) $\hat{\rho} = e^{-\beta\hat{H}}/Z$ using the NRG approximation Eq. (3),

$$\hat{\rho} \simeq \sum_n \sum_{se} |se\rangle^D_n \frac{e^{-\beta E^n_s}}{Z}{}^D_n\langle se| = \sum_n w_n \hat{\rho}^{[n]}_{DD}, \tag{8}$$

where $w_n \equiv d^{N-n}Z^D_n/Z$ and $Z^D_n \equiv \sum_s^D e^{-\beta E^n_s}$. The RHS of Eq. (8) expresses $\hat{\rho}$ as sum over $\hat{\rho}^{[n]}_{DD}$, the density matrix for the *discarded* states of shell n, properly normalized as $\mathrm{Tr}[\hat{\rho}^{[n]}_{DD}] = 1$, and entering with relative weight w_n, with $\sum_n w_n = 1$. Similarly, for spectral functions we have

$$\langle\ldots\rangle_T = \sum_n w_n\langle\ldots\rangle_n, \qquad \mathcal{A}(\omega) = \sum_n w_n \mathcal{A}_n(\omega), \tag{9}$$

where the averages $\langle\cdots\rangle_n$ and spectral functions $\mathcal{A}_n(\omega)$ are calculated with respect to $\hat{\rho}^{[n]}_{DD}$ of shell n only.

Previous strategies [4–11] for thermal averaging amount to using a "single-shell approximation" $w_n = \delta_{nN_T}$ for the density matrix and terminating the chain at a length $N = N_T$ set by $T \simeq \Lambda^{-1/2(N_T-1)}$. As a result, spectral features on scales $\omega \le T$, which would require a longer chain, are described less accurately [see Figs. 2(a) and 2(b)]. Our

novel approach avoids these problems by using the *full* density matrix (FDM), summed over *all* shells, letting the weighting function w_n select the shells relevant for a given temperature yielding a smooth T dependence [see Fig. 2(c)]. Since w_n has a peak width of five to ten shells depending on Λ, d and M_K and peaks at n values somewhat above N_T [arrow Fig. 2(b)], spectral information from energies well below T is retained.

Let us now consider the spectral function $\mathcal{A}^{\mathcal{BC}}(\omega)$, for local operators $\hat{\mathcal{B}}$ and $\hat{\mathcal{C}}$. Equations (4), (6), (8), and (9) can be used to evaluate $\langle\hat{\mathcal{B}}(t)\hat{\mathcal{C}}\rangle_n$. Fourier transforming the result we find (sums over ss' and σ_n implied)

$$\mathcal{A}_n^{\mathcal{BC}}(\omega) = \sum_{m>n_0}^{n} \sum_{XX'}^{\neq KK} [\mathcal{C}^{[m]}_{X'X}\rho^{[mn]}_{XX}]_{s's}[\mathcal{B}^{[m]}_{XX'}]_{ss'}\delta(\omega - E^m_{s's}),$$

$$[\rho^{[m=n]}_{DD}]_{ss'} = \delta_{ss'}\frac{e^{-\beta E^n_s}}{Z_n}, \tag{10}$$

$$[\rho^{[m<n]}_{KK}]_{ss'} = [A^{[\sigma_{m+1}]}_{KK}\ldots A^{[\sigma_n]}_{KD}\rho^{[nn]}_{DD}A^{[\sigma_n]\dagger}_{DK}\ldots A^{[\sigma_{m+1}]\dagger}_{KK}]_{ss'}.$$

Similarly, the static quantity $\langle\hat{\mathcal{B}}\hat{\mathcal{C}}\rangle_n$ equals the first line's RHS without the δ function. The matrix elements $[\rho^{[mn]}_{XX}]_{ss'} \equiv \sum_{em}^{X}\langle se|\hat{\rho}^{[n]}_{DD}|s'e\rangle^X_m$ are given by the second and third lines, together with $\rho^{[m=n]}_{KK} = \rho^{[m<n]}_{DD} = 0$. After performing a "forward run" to generate all relevant NRG eigenenergies and matrix elements, $\mathcal{A}^{\mathcal{BC}}(\omega)$ can be calculated in a single "backward run," performing a sum with the structure $\sum_{m>n_0}^{N}[\mathcal{C}\rho^{\rm red}\mathcal{B}\cdot\delta()]^{[m]}$, starting from $m = N$. Here $\rho^{[m],\rm red}_{XX} \equiv \sum_{n\geq m}^{N} w_n\rho^{[mn]}_{XX}$ (updated one site at a time during the backward run) is the *full* reduced density matrix for shell m, obtained iteratively by tracing out all shells at smaller scales $\Lambda^{-n/2}$ ($n \geq m$).

Equations (8)–(10) are the main results of our "FDM-NRG" approach. They rigorously generalize Hofstetter's DM-NRG [8] (which leads to similar expressions, but using $w_n = \delta_{nN_T}$ and without excluding KK matrix elements), and provide a concise prescription, free from double-counting ambiguities, for how to combine NRG data from different shells when calculating $\mathcal{A}^{\mathcal{BC}}(\omega)$. The relevant sum rule is satisfied *identically*, since by construction $\int d\omega\,\mathcal{A}^{\mathcal{BC}}_n(\omega) = \langle\hat{\mathcal{B}}\hat{\mathcal{C}}\rangle_n$ holds for every n and arbitrary temperature and NRG parameters Λ and M_K.

Smoothing discrete data.—We obtain smooth curves for $\mathcal{A}^{\mathcal{BC}}(\omega)$ by broadening the discrete δ functions in Eq. (10) using a broadening kernel that smoothly interpolates from a log-Gaussian form (of width α) [2,4] for $|\omega| \gtrsim \omega_0$, to a regular Gaussian (of width ω_0) for $|\omega| < \omega_0$, where ω_0 is a "smearing parameter" whose significance is explained below. To obtain high-quality data, we combine small choices of α with an average over N_z slightly shifted discretizations [3] (see [13] for more details).

Application to Anderson model.—We illustrate our method for the standard single-impurity Anderson model (SIAM). Its local Hamiltonian $\hat{h}_0 \equiv \sum_\sigma \epsilon_0 c^\dagger_{0\sigma}c_{0\sigma} +$

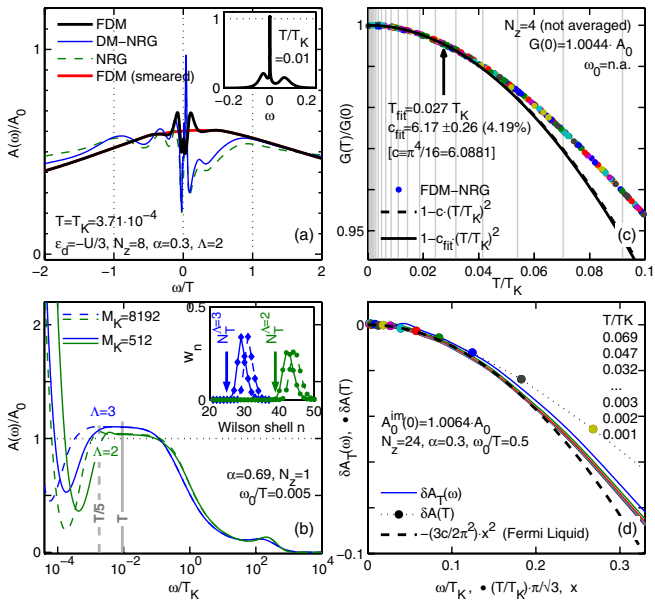

FIG. 2 (color online). FDM-NRG results for the spectral function $\mathcal{A}_T(\omega)$ of the SIAM, with $U = 0.12$, $\Gamma = 0.01$, $\epsilon_d = -U/2$ ($T_K = 2.185\times10^{-4}$), $\Lambda = 1.7$, and $M_K = 1024$, unless indicated otherwise. Inset of (a): FDM-NRG result for $A_T(\omega)$ with ω in units of bandwidth. For (a),(b), an unconventionally small smearing parameter was used, $\omega_0 = 0.005T$ [except for thick gray (red) curve in (a)], with $\omega_0 = 0.5T$), leading to spurious low-frequency oscillations. These illustrate the differences (a) between NRG (dashed green curve), DM-NRG [solid thin (blue) curve), and FDM-NRG (black curve) results for the regime $\omega \lesssim T$, and (b) between different choices of M_K and Λ for FDM-NRG, which yield different shapes for the weights w_n [shown in inset of (b)]: larger Λ reduces the scale δ_T at which oscillations set in, but yields less accurate values for the Kondo peak height in the regime $\delta_T \lesssim \omega \lesssim T_K$. (c),(d) Comparison of high-quality FDM-NRG data (dots, solid curves) with exact Fermi-liquid results (black dashed lines) for (c) the conductance $G(T)$ for $T \ll T_K$, and (d) for $\mathcal{A}^{\rm im}_T(\omega)$ for $T, \omega \ll T_K$. In (c), $c_{\rm fit}$ was found from a data fit to $c_{\rm fit}(T/T_K)^2$ for $T < T_{\rm fit}$ (arrow). In (d) we plot $\delta\mathcal{A}_T(\omega) = [A^{\rm im}_T(\omega) - A^{\rm im}_T(0)]/A^{\rm im}_0(0)$ vs ω/T_K (curves) and $\delta\mathcal{A}(T) = [A^{\rm im}_T(0)/A^{\rm im}_0(0) - 1]$ vs $(T/T_K)\pi/\sqrt{3}$ (dots), for a set of 12 temperatures between 0.001 and $0.069T_K$ (with curves and dots having same T in the same color), to illustrate the leading ω and T behavior of $\mathcal{A}^{\rm im}_T(\omega)$; the dashed black line represents the expected Fermi-liquid behavior in both cases, $-(3c/2\pi^2)x^2$ vs x.

$Uc^\dagger_{0\uparrow}c_{0\uparrow}c^\dagger_{0\downarrow}c_{0\downarrow}$ describes a localized state with energy ϵ_0, with a Coulomb penalty U for double occupancy. It is coupled to a Wilson chain $\sum_{n\sigma}\lambda_n(c^\dagger_{n+1\sigma}c_{n\sigma} + \text{H.c.})$, which generates a local level width Γ. We calculated $\mathcal{A}^<(\omega) \equiv \mathcal{A}^{c^\dagger_{0\sigma}c_{0\sigma}}(-\omega)$, $\mathcal{A}^>(\omega) \equiv \mathcal{A}^{c_{0\sigma}c^\dagger_{0\sigma}}(\omega)$ and $\mathcal{A} \equiv \mathcal{A}^> + \mathcal{A}^<$. An "improved" version $\mathcal{A}^{\rm im}$ thereof can be obtained by calculating the impurity self-energy $\Sigma(\omega, T)$ [6,13] via FDM-NRG, which is less sensitive to smoothening details and yields more accurate results for the Kondo peak height $\mathcal{A}_{T\simeq0}(0)$ at zero temperature.

Sum rules.—As expected, we find FDM-NRG to be significantly more accurate at lower computational cost

than NRG or DM-NRG [8,15]. The sum rules

$$\int d\omega\, \mathcal{A}^{c^\dagger_{0\sigma} c_{0\sigma}}(\omega) = \langle c^\dagger_{0\sigma} c_{0\sigma}\rangle_T, \quad \int d\omega\, \mathcal{A}(\omega) = 1 \quad (11)$$

hold exactly to 10^{-15} for our discrete data, and to 10^{-4} after smoothing (due to numerical integration inaccuracies). Moreover, even for M_K as small as 256, our results for $\mathcal{A}_{T\simeq 0}(0)$ and $\mathcal{A}^{\mathrm{im}}_{T\simeq 0}(0)$ typically agree to within 2% and 0.2%, respectively, with the Friedel sum rule, which requires $\pi\Gamma\mathcal{A}^{\mathrm{exact}}_{T=0} = \sin^2\pi\langle c^\dagger_{0\sigma} c_{0\sigma}\rangle_0$. The exact relation $\mathcal{A}^<(\omega) = f(\omega)\mathcal{A}(\omega)$ (f is the Fermi function), which follows from detailed balance, is likewise satisfied well (though not rigorously so): the left-hand side of Eq. (11) typically equals $\int d\omega f(\omega)\mathcal{A}(\omega)$ to better than 10^{-4}.

Low-frequency data.—Because of the underlying logarithmic discretization, all NRG-based schemes for calculating finite-temperature spectral functions inevitably produce spurious oscillations at very low frequencies $|\omega| \ll T$. The scale δ_T at which these set in can be understood as follows: the Lehmann sum in Eq. (1) is dominated by contributions from initial states $|a\rangle$ with energy $E_a \simeq T$, represented by NRG shells with n near N_T. The characteristic energy scale of these states limits the accuracy obtainable for energy differences E_{ba} to accessible final states $|b\rangle$. Thus the scale δ_T is set by those shells which contribute with largest weight w_n to the density matrix.

We analyze this in more detail in Figs. 2(a) and 2(b) by purposefully choosing the smearing parameter to be unconventionally small, $\omega_0 \ll T$. The resulting spurious oscillations are usually smeared out using $\omega_0 \gtrsim \delta_T$ [Fig. 2(a), thick gray (red) curve], resulting in quantitatively accurate spectral functions only for $|\omega| \gtrsim \omega_0 \simeq \delta_T$. For conventional NRG approaches, the "single-shell" approximation $w_n = \delta_{nN_T}$ typically leads to $\delta_T \simeq T$, as can be seen in Fig. 2(a) [dashed (green) line and thin solid (blue) line]. In contrast, FDM-NRG yields a significantly reduced value of $\delta_T \simeq T/5$ [Fig. 2(a), black line, and Fig. 2(b)], since the weighting functions w_n [inset of Fig. 2(b)] retain weight over several shells below N_T, so that lower-frequency information is included.

Fermi-liquid relations.—To illustrate the accuracy of our low-frequency results, we calculated $\mathcal{A}^{\mathrm{im}}_T(\omega)$ for $\omega, T \ll T_K$ for the symmetric SIAM, and made quantitative comparisons to the exact Fermi-liquid relations [14],

$$A_T(\omega) \simeq A_0\left[1 - \frac{c}{2}\left(\frac{T}{T_K}\right)^2 - \frac{3c}{2\pi^2}\left(\frac{\omega}{T_K}\right)^2\right],$$

$$G(T) \equiv \int_{-\infty}^{\infty} d\omega A(\omega, T)\left(-\frac{\partial f}{\partial \omega}\right) \simeq A_0\left[1 - c\left(\frac{T}{T_K}\right)^2\right].$$

Here $A_0 \equiv 1/\pi\Gamma$, $c \equiv \pi^4/16$, and the Kondo temperature T_K is defined via the static magnetic susceptibility [4] $\chi_0|_{T=0} \equiv 1/4T_K$. Figures 2(c) and 2(d) show the FDM-NRG data [gray (colored) dots and lines] to be in remarkably good quantitative agreement with these relations (black dashed curves). The results for the "conductance" $G(T)$, being a frequency integrated quantity obtained by summing over discrete data directly without the need for broadening, are more accurate than for $\mathcal{A}^{\mathrm{im}}_T(\omega)$, and reproduce the prefactor c with an accuracy consistently within 5% (until now, accuracies of the order of 10%–30% had been customary). The smoothness of the data in Fig. 2(c), obtained using temperatures not confined to the logarithmic grid $\Lambda^{-n/2}$ [gray vertical lines in Fig. 2(b)], together with the remarkable stability with respect to different z shifts illustrate the accuracy of our approach.

Conclusions.—Our FDM-NRG method offers a transparent framework for the calculation of spectral functions of quantum impurity models, with much improved accuracy at reduced complicational cost. Its results satisfy frequency sum rules rigorously and give excellent agreement with other consistency checks such as the Friedel sum rule, detailed balance, or Fermi-liquid relations, including the regime $\omega \lesssim T$.

We thank F. Anders, R. Bulla, T. Costi, T. Hecht, W. Hofstetter A. Rosch, and G. Zárand for discussions, and the KITP in Santa Barbara for its hospitality. The work was supported by DFG (No. SFB 631 and No. De-730/3-1,3-2), and in part by the NSF (No. PHY99-07949).

Note added.—Just before completion of this work we learned that Peters, Pruschke, and Anders had followed up on the same idea [15].

[1] K. G. Wilson, Rev. Mod. Phys. **47**, 773 (1975); H. R. Krishnamurti, J. W. Wilkins, and K. G. Wilson, Phys. Rev. B **21**, 1003 (1980); **21** 1044 (1980).
[2] O. Sakai, Y. Shimizu, and T. Kasuya, J. Phys. Soc. Jpn. **58**, 3666 (1989).
[3] M. Yoshida, M. A. Whitaker, and L. N. Oliveira, Phys. Rev. B **41**, 9403 (1990).
[4] T. A. Costi, A. C. Hewson, and V. Zlatic, J. Phys. C **6**, 2519 (1994).
[5] T. A. Costi, Phys. Rev. B **55**, 3003 (1997).
[6] R. Bulla, A. C. Hewson, and T. Pruschke, J. Phys. C **10**, 8365 (1998).
[7] R. Bulla, T. Costi, and T. Pruschke, arXiv:cond-mat/0701105.
[8] W. Hofstetter, Phys. Rev. Lett. **85**, 1508 (2000).
[9] R. Bulla, T. A. Costi, and D. Vollhardt, Phys. Rev. B **64**, 045103 (2001).
[10] R. Bulla, N. H. Tong, and M. Vojta, Phys. Rev. Lett. **91**, 170601 (2003).
[11] F. B. Anders and A. Schiller, Phys. Rev. Lett. **95**, 196801 (2005); Phys. Rev. B **74**, 245113 (2006).
[12] F. Verstraete *et al.*, arXiv:cond-mat/0504305.
[13] See EPAPS Document No. E-PRLTAO-99-025733 for appendices which give more details. For more information on EPAPS, see http://www.aip.org/pubservs/epaps.html.
[14] A. Hewson, *The Kondo Problem to Heavy Fermions* (Cambridge University Press, New York, 1993).
[15] R. Peters, T. Pruschke, and F. B. Anders, Phys. Rev. B **74**, 245114 (2006). We recommend this paper for a more detailed comparison of the new and previous approaches.

APPENDIX

Smoothing Discrete Data:— The FDM-NRG yields the spectral function in the form of a Lehmann sum over discrete δ-functions, which have to be broadened to obtain a smooth function. Ideally, this should be done using a procedure for which the results are independent both of the parameters used for broadening and for discretizing the conduction band.

We calculate the smoothened spectral function using $\mathcal{A}(\omega) \equiv \int d\omega' K(\omega,\omega')\,\mathcal{A}_{\rm raw}(\omega')$. Here $\mathcal{A}_{\rm raw}(\omega') = \sum_n w_n \mathcal{A}_n(\omega')$ represents the discrete numerical data obtained from Eq. (10), which in practice we collect in binned form, typically using 250 bins per decade in ω', so that $\int d\omega'$ becomes a sum over bins. The raw data is folded with the broadening kernel $K(\omega,\omega')$, which we choose to be of the following form:

$$K(\omega,\omega') = L(\omega,\omega')h(\omega') + G(\omega,\omega')[1-h(\omega')] \quad (14a)$$

where

$$L(\omega,\omega') = \frac{\theta(\omega\omega')}{\sqrt{\pi}\alpha|\omega|} e^{-\left(\frac{\log|\omega/\omega'|}{\alpha}-\gamma\right)^2} \quad (14b)$$

$$= \frac{\theta(\omega\omega')}{\sqrt{\pi}\alpha|\omega'|} e^{-\left(\frac{\log|\omega'/\omega|}{\alpha}+\gamma-\frac{\alpha}{2}\right)^2} e^{-\alpha(\gamma-\frac{\alpha}{4})} ,$$

$$G(\omega,\omega') = \frac{1}{\sqrt{\pi}\omega_0} e^{-\left(\frac{\omega-\omega'}{\omega_0}\right)^2} , \quad (14c)$$

$$h(\omega') = \begin{cases} 1 , & |\omega'| \geq \omega_0 , \\ e^{-\left(\frac{\log|\omega'/\omega_0|}{\alpha}\right)^2} , & |\omega'| < \omega_0 . \end{cases} \quad (14d)$$

The chosen kernel K constitutes a smooth interpolation, of somewhat arbitrary shape $h(\omega')$, between a log-Gaussian [2, 4] broadening kernel L on the one hand, used for all ω'-frequencies but the smallest (with ω and ω' restricted to have the same sign); and a Gaussian broadening kernel G of width ω_0 on the other, used for $|\omega'| < \omega_0$ to smoothly connect the regimes of positive and negative frequencies. We choose ω_0 to be roughly a factor of 2 smaller than the smallest energy scale in the problem, including the Kondo temperature T_K (note that by construction in Eq. (14d) the transition to regular Gaussian sets in *below* ω_0).

The log-Gaussian kernel $L(\omega,\omega')$ was purposefully chosen to have the following three desirable features:
(i) *Frequency-dependent width:* being Gaussian on a logarithmic scale, on a linear scale its width as function of ω is proportional to ω'. This is needed to deal with the fact that spectral data generated using Wilson's logarithmic discretization grid is more coarse-grained at large frequencies than at smaller ones.
(ii) *Conservation of weight:* we have $\int d\omega L(\omega,\omega') = 1$, ensuring that $\int d\omega \mathcal{A}(\omega) = \int d\omega' \mathcal{A}_{\rm raw}(\omega')$.
(iii) *Conservation of peak height:* for the choice $\gamma = \alpha/4$ (adopted henceforth) L is *symmetric* under $\omega \leftrightarrow \omega'$, so that also $\int d\omega' L(\omega,\omega') = 1$. This ensures that the logarithmic broadening kernel maps a constant function onto itself (if $\mathcal{A}_{\rm raw}(\omega') = \mathcal{A}_0$, then $\mathcal{A}_{\rm raw}(\omega) = \mathcal{A}_0$), and thus does not change the height of a peak whose width on a logarithmic scale is broader than α. (In this respect our L differs from that of [2, 4, 15].)

Since choice (iii) implies that our log-Gaussian Kernel, as function of ω, describes a peak asymmetric w.r.t. ω' (shifted by $\alpha/4$ on a log scale), on a linear ω-scale the broadened data is stretched relative to the raw data by factor $e^{\alpha^2/4}$. This effect can be minimized by keeping α as small as possible. The smoothening of plain NRG data typically requires $\alpha \sim 1/\sqrt{\Lambda}$ (e.g. 0.7 for $\Lambda = 2$). However, smaller values (*e.g.* $\alpha \leq 0.3$ or even smaller) can be achieved by using the "z-trick" [3]: collect several (say N_z) sets of discrete FDM-NRG data, each obtained from a different, slightly shifted logarithmic grid $\{\Lambda^{-n-z}\}$ of discrete frequencies, for N_z different values of z between -0.5 and 0.5, and average the results. The hopping matrix elements along the Wilson chain are recalculated for each z by carefully tridiagonalizing the underlying logarithmically discretized Hamiltonian.

Self-energy representation:— The accuracy of the results for $\mathcal{A}_\sigma(\omega)$ for the Anderson model can be improved by expressing it in terms of the impurity self energy [6]: first, note that $\mathcal{A}_\sigma(\omega) = -{\rm Im}[\mathcal{G}^R_\sigma(\omega)]/\pi$, where $\mathcal{G}^R_\sigma(\omega)$ is the Fourier transform of $\mathcal{G}^R_\sigma(t) = -i\theta(t)\langle\{c_{0\sigma}(t), c^\dagger_{0\sigma}\}\rangle_T$. An improved version for $\mathcal{G}^R_\sigma(\omega)$ can be obtained by expressing it as

$$\mathcal{G}^{\rm im}_\sigma(\omega) = \frac{1}{\omega - \Delta_\sigma(\omega) - \Sigma^U_\sigma(\omega)}, \quad \Sigma^U_\sigma(\omega) = U\frac{\mathcal{F}^R_\sigma(\omega)}{\mathcal{G}^R_\sigma(\omega)}.$$

Here $\Delta_\sigma(\omega)$, the U-independent part of the self energy which characterizes the level's broadening, can be computed exactly, $\mathcal{G}^R_\sigma(\omega)$ is the standard ("non-improved") version of the correlator, and $\mathcal{F}^R_\sigma(\omega)$ is the Fourier transform of $-i\theta(t)\langle\{[c^\dagger_{0-\sigma}c_{0-\sigma}c_{0\sigma}](t), c^\dagger_{0\sigma}\rangle_T$.

We calculate the imaginary parts of $\mathcal{G}^R_\sigma(\omega)$ and $\mathcal{F}^R_\sigma(\omega)$ using FDM-NRG from Lehmann representations of the form (10), smoothen the discrete data as described above, Kramers-Kronig transform the smoothened results to obtain their real parts, and finally calculate $\Sigma^U_\sigma(\omega)$. Small wavy features in $\mathcal{G}^R_\sigma(\omega)$ and $\mathcal{F}^R_\sigma(\omega)$ that reflect the logarithmic discretization grid largely cancel out in the ratio $\Sigma^U_\sigma(\omega)$. Thus, smooth results for $\mathcal{G}^{\rm im}_\sigma(\omega)$ and $\mathcal{A}^{\rm im}_\sigma(\omega)$ can be obtained using much less (or even no) z-trick averaging, thus reducing the number of distinct FDM-NRG runs required to get good results. Moreover, since $\Sigma^U_\sigma(\omega \to 0)$ at $T = 0$ is found to approach 0, the self-energy representation also improves the accuracy with which the Friedel sum rule is fulfilled.

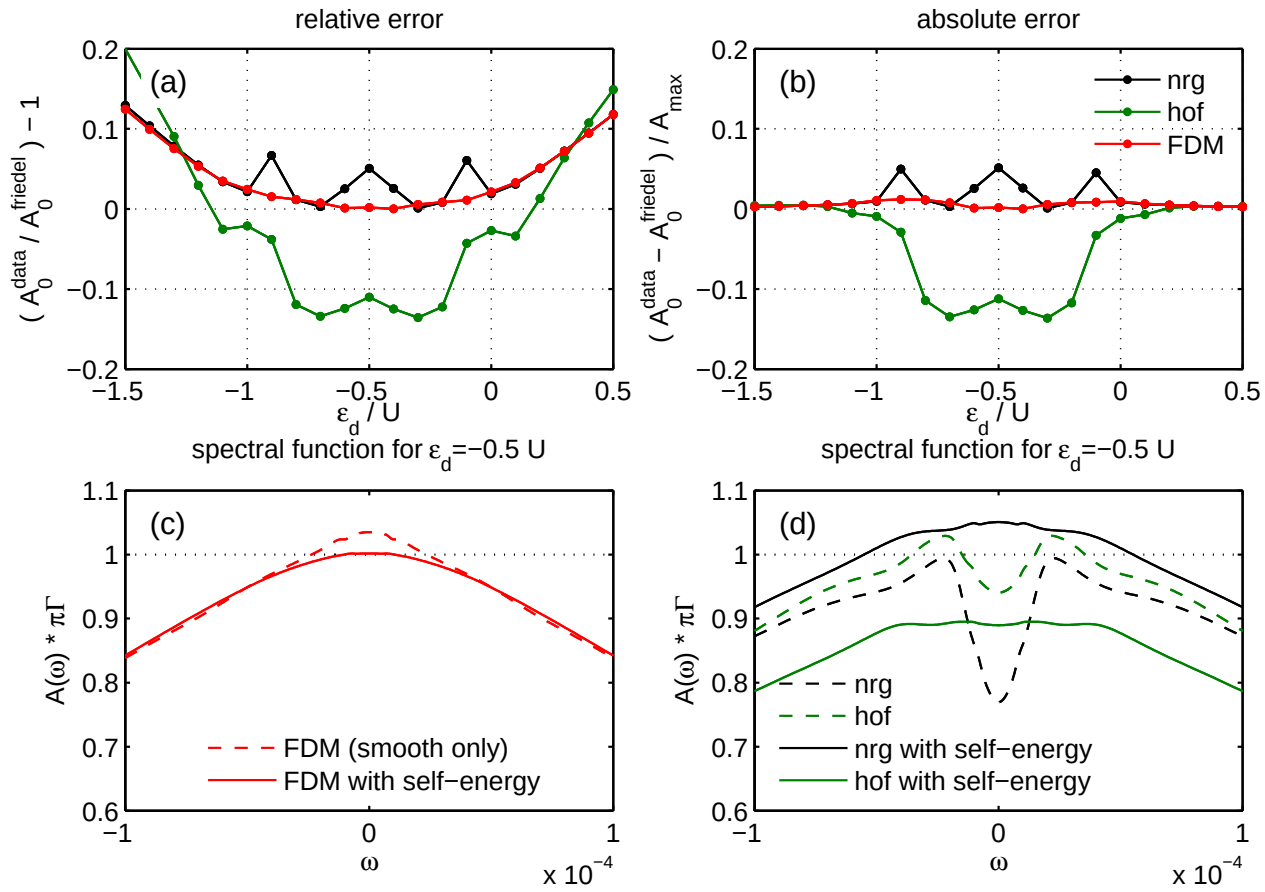

FIG. 1: Comparison of the Friedel sum rule of our FDM-NRG to the previous methods of plain NRG ('nrg') and Hofstetter's DM-NRG ('hof'). This is done for the same model parameters as in our paper while sweeping the onsite energy ϵ_d ($\Lambda = 2$, $M_K = 256$, $N_z = 8$, $\alpha = 0.3$, $U = 0.12$, $\epsilon_d = -U/2$, $\Gamma = 0.01$, $B = 0$ and $T_K = 2.2\,10^{-4}$). Panel (a) Relative error of the Friedel sum rule. Panel (b) – Absolute error with respect to maximum peak height of full spectral function $A_{\max}$. Panels (c) and (d) show a zoom into the spectral function around $\omega = 0$ for the symmetric point $\epsilon_d = -U/2$ for the methods presented in our paper (panel c) and for the previous methods (panel d), respectively.

Friedel Sum Rule:— The Friedel sum rule $A(0) = \sin^2(n_0\pi/2)/\pi\Gamma$ is a well known analytic result that is exact at zero temperature and can be used to check our data. Figure 1 shows a comparison of our method for calculating spectral functions to previous methods. As will be seen our method clearly leads to more accurate agreement with the Friedel sum rule for arbitrary parameter combinations. Since we know the dot occupancy n_0 numerically from our FDM-NRG method, we compare the actual value of our spectral function at $\omega = 0$ to the expected value predicted by Friedel sum rule. We do this for our FDM-NRG method, but also for the older versions of plain NRG ('nrg' in Fig. 1 and Hofstetter's DM-NRG ('hof'). In all three cases, the spectral function was calculated using the self-energy representation (Ref [6]) as outlined in the Appendix of our paper.

Panels 1a and 1b show the comparison for the single impurity Anderson model (the same as used in our paper), but here for a whole sweep of the onsite energy ϵ_d. Figure 1a shows the relative error of $A(\omega = 0)$ with respect to the value expected from the Friedel sum rule. Figure 1b shows the same data, but normalized with respect to the maximum of the full spectral function. This is just to show that the increase of the error as ϵ_d is changed from its value -0.5 (the symmetry point of the model) seen in Fig. 1a is due to fact that absolute value of $A(\omega = 0)$ then becomes smaller, because the dominant peak then shifts increasingly further away from $\omega = 0$.

All data in Figure 1 were obtained using *exactly the same* broadening procedure as described in the attachment to our paper. for the discrete data obtained from the three different methods. The origin of the artificial oscillations in the error for the previous methods ('nrg' and 'hof' in the figure) can be easily understood by looking at the underlying smooth spectral functions that were used to obtain Figs. 1a and 1b. For $\epsilon_d = -0.5\,U$ a zoom into the spectral function is shown around $\omega = 0$ for FDM-NRG in Fig. 1c and for the other methods in Fig. 1d. The solid lines are the smoothened discrete data, the dashed curves the subsequently improved data using self-energy (Ref [6]). Evidently, the data in Fig. 1d shows problematic artifacts (dips and other oscillations) not present in Fig. 1c.

Of course, the broadening parameters employed here could have been chosen such that the previous methods ('nrg' and 'hof' in the figure) also yield more satisfactory results, in that the data around $\omega = 0$ could have been 'tailored' to look smoother by using a few crutches such as increased broadening parameter α. However, we did not do that here to emphasize the greatly improved quality of our FDM-NRG approach compared to standard NRG and DM-NRG. Clearly, FDM-NRG gives the best data quality throughout.